



# STUDY ON THE DETERIORATION OF SHEAR CAPACITY AND FAILURE MODE OF RC COLUMNS SUBJECTED TO HIGH VARYING AXIAL FORCE

JPH Toxqui<sup>(1)</sup>, A Tasai<sup>(2)</sup>, K Sugimoto<sup>(3)</sup>, K Kusunoki<sup>(4)</sup>

<sup>(1)</sup> Graduate Student, Institute of Urban Innovation, Yokohama National University, [ic\\_toxqui@hotmail.com](mailto:ic_toxqui@hotmail.com)

<sup>(2)</sup> Prof., Institute of Urban Innovation, Yokohama National University, [tasai@ynu.ac.jp](mailto:tasai@ynu.ac.jp)

<sup>(3)</sup> Assoc. Prof., Institute of Urban Innovation, Yokohama National University, [kuniyoshi-sugimoto@ynu.ac.jp](mailto:kuniyoshi-sugimoto@ynu.ac.jp)

<sup>(4)</sup> Assoc. Prof., Earthquake Research Institute, The University of Tokyo, [kusunoki@eri.u-tokyo.ac.jp](mailto:kusunoki@eri.u-tokyo.ac.jp)

## Abstract

This paper was written about the deterioration of the shear strength capacity and the failure mode of columns subjected to high fluctuation axial force. Four columns designed to avoid shear failure and develop high ductility were tested under different levels of varied axial force and in unidirectional cyclic lateral loading. The failure mode is explained through the deformation behavior of the different portions all over the height of the column. Plastic analysis was employed to determine the deterioration of the shear capacity. The achieved results are as follows: in the failure mode, flexural behavior and ductility were satisfactorily developed; however, at a large lateral drift angle, the columns presented axial collapse and shear failure. The deterioration of the shear capacity was well predicted by the employed plastic analysis for these columns.

*Keywords: High axial force; RC column; high ductility; shear capacity; failure mode.*

## 1. Introduction

In the world, more and more tall buildings are being designed and built. For the lower stories of these buildings, the use of space becomes an important matter from the architectural point of view. Consequently, the cross sections of columns of those floors have to be reduced in order to achieve more useful space. The columns, located at the corners of this kind of buildings, are demanded to have a higher axial force than usual, especially during an earthquake. In these kind of columns, the structural behavior is highly important as well as the deterioration of the shear strength and the failure mode. Additionally, the effect of varied axial load during a seismic event is still uncertain and past experiments presented results that stand out the important effects of the varied axial force on the strength and ductility of columns [1].

This research studied the deterioration of shear strength capacity and the failure mode of four columns after the maximum peak of lateral strength. The columns, designed to avoid shear failure and develop large ductility, were tested under different levels of varied axial force subjected to reversal cyclic lateral loading. The design of the columns was done with the proposal normative for RC columns that carry axial force ratio up to 0.67 [2]. The study of the deformation behavior per different portions all over the height of the column was used to explain their failure mode. The deterioration of shear capacity was analyzed by the truss and arch mechanisms at the middle span of the columns.

There are two documents in the matter of the design of RC columns under high axial force in Japan. The first is The Technical Standard Manual Concerned on Buildings Structure (2007) [3] which has severe restrictions to classify columns as high ductile columns (FA). The second is the draft for “Calculation Standard for Horizontal Load-Carrying of Reinforced Concrete Structure” (For public comments) [2] recently issued by The Architectural Institute of Japan (AIJ) in 2015, where columns built with normal strength materials can develop ductility up to the drift angle of 2.5% under high axial force.



## 2. Test Plan

### 2.1 Outline of the specimens

In this study, the columns were designed to meet the requirements of reference [2]. Table 1 shows the requirements of columns to be classified as FA according to the applied axial force ratio ( $\eta$ ), where axial force ratio is defined by Eq. 1.

$$\eta = \frac{\sigma_0}{F_c} \quad (1)$$

Where,  $\sigma_0$ : axial stress in the column  $\sigma_0 = N/bD$  (MPa),  $N$ : axial force (N);  $b$ : width of the cross section (mm),  $D$ : height of the cross section (mm),  $F_c$ : specific compressive strength of concrete (MPa).

In Table 1, two levels of the axial force ratio are stated as:  $\eta \leq 0.45$  and  $0.45 < \eta \leq 0.67$  according to other parameters. The values of  $\eta$  in Table 1 correspond to the maximum value of the axial force ratio that the column can support at the ultimate state. In the design of the specimens, the shear reinforcement indicator (SRI) of Eq. 2 was larger than 1.0.

Table 1 – Requirements for FA columns 2015 [2].

Axial force ratio	SRI	$h_0 / D$	$p_g$ (%)	$\tau_u / F_c$	Notes
$\eta \leq 0.45$	Eq. (2)	$\geq 2.0$	--	$\leq 0.20$	--
$0.45 \leq \eta \leq 0.67$		$\geq 3.0$	$\geq 1.6$		*1

Where  $h_0$  is the height of the column (mm),  $p_g$  is the ratio of total reinforcement and  $\tau_u$  is the ultimate shear stress. \*1) In each direction of the cross section, two or more sub-ties should be placed. Four or more longitudinal reinforcing bars should be arranged in each face of the column. The spacing between transverse reinforcement should be less than 100mm and less than six times the smallest diameter of the longitudinal bars.

Shear reinforcement indicator (SRI) is determined as:

$$\frac{p_w \sigma_{ws} / v_0 F_c}{0.30(\eta)^2 + 0.10} \geq 1.0 \quad (2)$$

Where,  $p_w$ : shear reinforcement ratio,  $\sigma_{ws}$ : effective strength of shear reinforcement ( $\sigma_{ws} \leq 85\sqrt{F_c}$ ) (MPa),  $v_0$ : effective strength coefficient of concrete ( $v_0 = 1.7F_c^{-0.333}$ )

It was important that the columns did not fail in shear mode, for this reason the standard assumption to avoid shear failure was employed as Eq. 3 describes.

$$\frac{Q_{su}}{Q_{mu}} \geq 1.1 \quad (3)$$

Where:  $Q_{su}$  is the ultimate shear strength (N) and  $Q_{mu}$  is the ultimate flexural strength (N), more information about the equations to obtain these strengths can be found in the reference [2].

The first specimen, named as No.1, was designed to match all the requirements of Table 1 for  $\eta \leq 0.45$ . The rest of the specimens were named as No.2-A, No.2-B, and No.3 respectively, they were designed to match all the requirements of  $0.45 \leq \eta \leq 0.67$ . The second and third specimens were physically identical, the difference was the variation of the maximum axial force applied during the test, specimen No.2-A was loaded with axial force ratio of the design ( $\eta \leq 0.65$ ) and No.2-B with a lower one ( $\eta \leq 0.4$ ). The objective in this case was to compare the ductile behavior of these columns when the axial force demanded during an earthquake is lower than that of the design. Figure 1 shows the dimensions and arrangement of the bars of the cross section of all columns and the raised view of No.2-A and B. Table 2 shows the characteristics of the columns and employed materials.

### 2.1.1 Materials

The standard strengths of the materials (SS) and the actual strength of these material (AS) obtained from material tests are shown in Table 2.

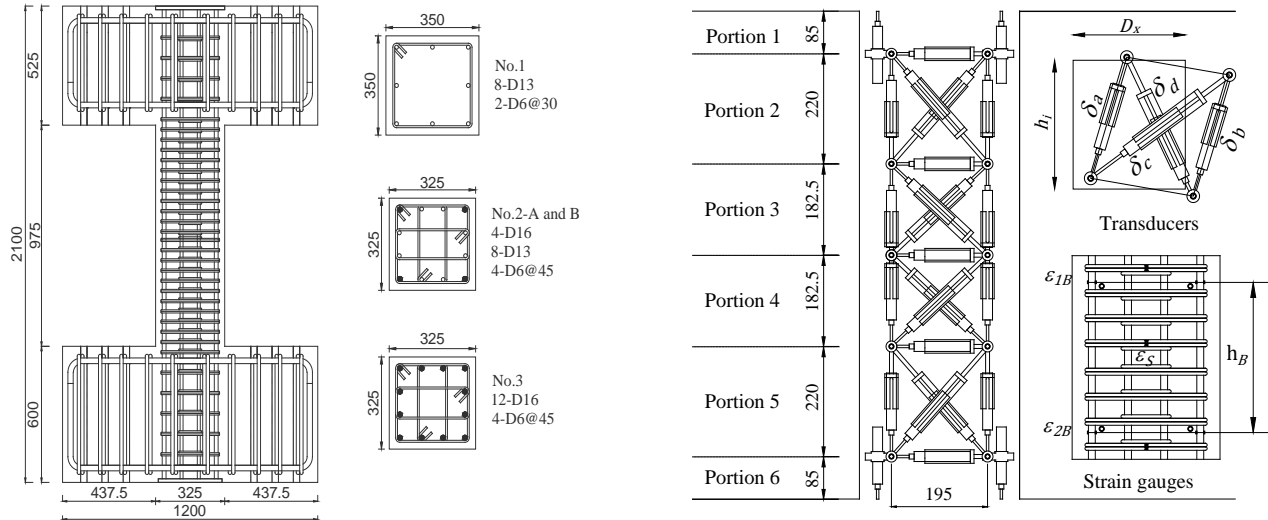


Figure 1 Reinforcement details of the specimens (mm)

Table 2 Characteristics of the columns and materials

Column	$h_0$	$b=D$	$F_C$	$\sigma_B$	$\sigma_y$		
	mm	mm			MPa	MPa	D13
No.1	1100	350	21	30.0	419	537	340
No.2-A	975	325		31.1			
No.2-B	975			30.7			
No.3	1100			29.8			

$\sigma_B$ : actual strength of concrete

$\sigma_y$ : strength of the longitudinal reinforcement

$\sigma_{wy}$ : strength of the transversal reinforcement

### 2.1.2 Instrumentation

The specimens were instrumented internally and externally to record the strain and deformations during the test. Internally, a pair of strain gauges sets were pasted in strategically points over the transversal and longitudinal reinforcement, the strain of each of these points was taken as the average of the strain recorded by both gauges. Externally, the columns were divided into six rectangular portions to place a set of transducers for the calculation of shear deformation. Figure 1 shows the placed transducers and details of the strain gauges in the columns No.2-A and No.2-B.

### 2.1.3 Test setup

Figure 2a shows the test setup of the specimens in the laboratory. Two hydraulic oil jacks of 1000kN were used to apply the axial force and to keep the top and bottom stubs of the specimens in parallel during the test. Two hydraulic oil jacks of 500kN were used to apply lateral force to the specimens. Load cells were placed in the hydraulic jacks to measure the acting force.

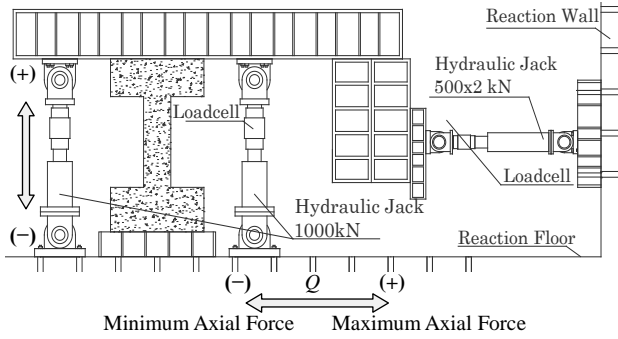


Figure 2a Test setup

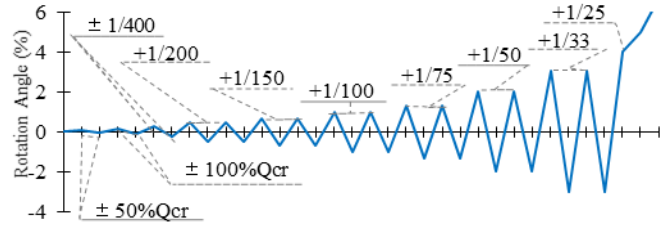


Figure 2b Lateral load history

## 2.2 Load history

Lateral and axial loads were simultaneously controlled during the test to simulate the seismic effect on columns.

### 2.2.1 Lateral load history

Figure 2b shows the applied lateral load history for all specimens. In the first two cycles, the lateral load was applied with force control and constant compressive axial force, which were, the cycles of  $\pm 50\%$  and  $\pm 100\%$  of the shear cracking strength ( $Q_{cr}$ ) given by Eq. 4 [2]. For the rest of the cycles of Figure 2b, the lateral force was controlled by displacement and the axial force was controlled according to the acting shear force at each step.

$$Q_{cr} = \left[ 1 + \frac{\sigma_0}{14.7} \right] \left\{ \frac{0.061(\sigma_0 + 49)}{\frac{M}{Q_d} + 1.7} \right\} b_j \quad (4)$$

$\frac{M}{Q_d}$ : shear span ratio ( $1 \leq \frac{M}{Q_d} \leq 3$ ). The values of  $Q_{cr}$  are listed in Table 3

### 2.2.2 Control of axial force ratio

The axial force was applied in terms of axial force ratio. For the cycles of  $\pm 50\%$  and  $\pm 100\%$  of  $Q_{cr}$  the applied compressive axial force ratio was constants. For the rest of the lateral load cycles, the axial force was controlled according to the measured shear force applied during the test by Eq. 5.

$$\eta_{applied} = \eta_i + \frac{Q}{Q_{su}} \Delta_\eta \quad (5)$$

Where,  $\eta_i$ : constant compressive axial force ratio,  $\Delta_\eta$ : increment of the axial force ratio,  $Q$ : measured shear force in each step during the test (N)

$\eta_i$  was 0.15 for column No.1 and 0.25 for the rest of the specimens.  $\Delta_\eta$  was equal to 0.3 for column No.1, 0.40 for column No.2-A, 0.15 for column No.2-B, and 0.37 for column No.3. During the test, the applied axial force ratio was limited to the maximum value of  $\eta_i + \Delta_\eta$  and minimum value of  $\eta_i - \Delta_\eta$  in all columns. The applied compressive axial forces (N) in function of the measured shear force are shown in Table 3.

The maximum axial force ratio was applied at the same time when the positive lateral load was applied, and the minimum axial force ratio was applied at the same time when the reversal (negative) lateral load was applied. The direction of the lateral load is illustrated in Figure 2a. The Figure 3 shows the relationship between the axial force ratio and the lateral force, the computed values of  $Q_{su}$  and  $Q_{mu}$  were plotted with the axial force



ratio in terms of  $\eta$ . In this figure, is important to notice that for column No.2-B the shear force reaches the shear strength before the flexural strength.

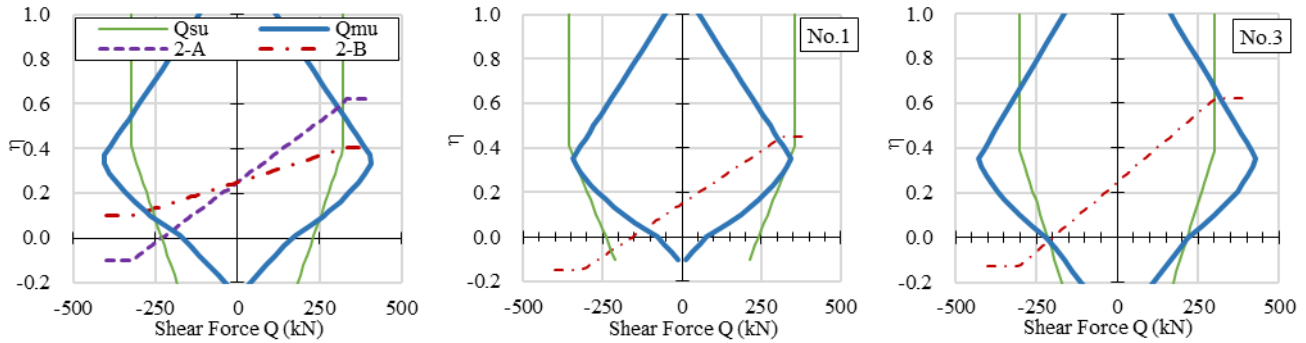


Figure 3 Applied axial force ratio and shear force relationship

Table 3 – Summary of specimens (Units: mm, kN)

Col.	$h_0 / D$	$p_g$ %	$p_t$ %	$p_w$ %	$\sigma_0 / F_c$	$\sigma_0 / \sigma_B$	N kN	SRI		$Q_{su} / Q_{mu}$		$\tau_u / F_c$		$Q_{cr}$ AS	*2
								SS	AS	SS	AS	SS	AS		
No.1	3.1	0.83	0.31	0.60	0.45	0.45	1714	1.0	0.75	1.10	1.00	0.12	0.10	200	FB
No.2-A	3.0	1.71	0.86	0.87	0.66	0.65	2135	1.0	0.77	1.17	1.12	0.12	0.12	210	FD
No.2-B					0.66	0.40	1279	1.0	1.20	1.17	0.80	0.12	0.13	143	
No.3	3.4	2.26	1.13	0.66	0.62	1951	1.0	0.84	1.00	0.94	0.12	0.14	177		

\*2 stiffness classification according to The Technical Standard Manual Concerned on Buildings Structure (2007) [3]

### 3 Test results and discussion

#### 3.1 Failure mode

##### 3.1.2 Hysteresis behavior

In Figure 4, the hysteresis characteristics of the columns are shown as the relationship between shear force and the lateral drift angle ( $R$ ). The ultimate lateral drift angle ( $R_u$ ) was defined as the lateral drift angle when the shear force of the specimens decreased down to 80% of the maximum strength during the test ( $Q_{max}$ ). The ductility performance of the column would be considered satisfactory when  $R_u$  is larger than 2.5%. The ultimate drift angle is marked for each specimen; these values were to 3.0%, 3.4%, 6.2%, and 4.4% for the columns on their respective order. It can be said that the columns reached the expected ductility performance.

Figure 4 also shows the lateral drift angles when the reinforcement yielded. For all columns, rebar yielded in compression around the lateral drift angle of 0.6% and hoops yielded approximately at the lateral drift angle of 2%. After hoops started to yielding, rebar yielded in tension for the columns No.2-A and No.3 (columns where  $\eta > 0.6$ ). For column No.1, rebar yielded in tension before the yielding of hoops and for No.2-B, rebar and hoops yielded in tension at the same lateral drift angle (2%). Due to the fact that, rebar started to yield before than the hoops did, it can be assumed that flexural behaviors were dominant for all columns.

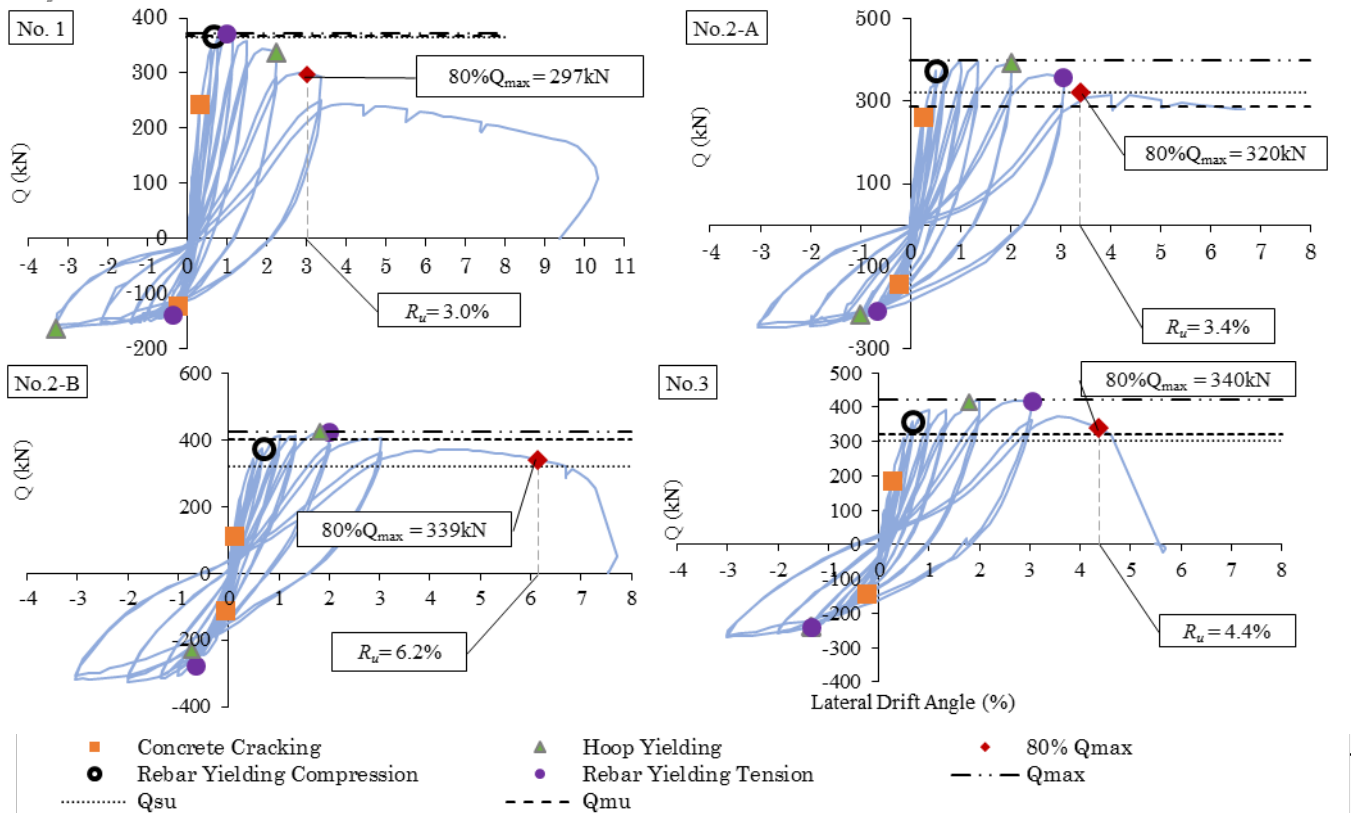


Figure 4 Hysteresis characteristics of the columns

### 3.2 Deformation behavior in each portion

In order to explain the failure behavior of the specimens, four types of data related to the deformations are presented.

The first data corresponds to the global axial deformation ( $\delta_{ac}$ ) obtained according to equation 6 which data were recorded by two transducers placed between the upper and lower concrete stubs of the specimens. These data are presented in Figure 5 as a continuous line.

$$\delta_{ac} = \frac{\bar{\delta}}{h_0} \quad (6)$$

Where:  $\bar{\delta}$  is the average axial displacement recorded by the vertical transducers

On the second type, the axial deformation ( $\delta_{ap}$ ) was obtained according to equation 7 from 12 vertical transducers. The position of these transducers on the column was presented in Figure 1.

$$\delta_{ap} = \frac{1}{h_0} \sum_i^n \frac{\delta_a + \delta_b}{2} \quad (7)$$

Where:  $\delta_a$  and  $\delta_b$  correspond to the vertical transducers shown in the detail in Figure 1. These data are presented in Figure 5 with a dashed line.

On the third type of data, the axial deformation in compression per each portion ( $\delta_{api}$ ) is presented according to equation 8.



$$\delta_{\alpha Pi} = \frac{\delta_{\alpha} + \delta_{\beta}}{2} \frac{1}{h_i} \quad (8)$$

Where:  $h_i$  is the height of each portion. The axial deformation per each portion is shown in Figure 6.

The fourth data shows the shear deformation ( $\delta_v$ ) obtained from the diagonal set of eight transducers from portion 2 to portion 5 (Figure 1) according to the equation 9.

$$\delta_v = \frac{1}{4h_i D_x} (\delta_d - \delta_c)(2l_{\alpha} + \delta_d + \delta_c) \quad (9)$$

Where:  $\delta_d$  and  $\delta_c$  the diagonal transducers shown in detail in Figure 1.  $\delta_v$  is shown in Figure 7.

In the following paragraphs, the axial deformation behavior is shown by the displacement peaks of the lateral load history. The positive direction of the lateral force, where the lateral drift angle is positive and the applied axial force was high compression, will be only described from now on.

Figure 5 shows the total axial deformation derived from Eq. 6 and 7. The comparison of the global axial deformation ( $\delta_{\alpha G}$ ) and the axial deformation obtained from portions ( $\delta_{\alpha P}$ ) shows a similar tendency on the behavior of the axial deformation of all specimens. For that reason, it is considered that the addition of axial deformations for all portions in equation 7 in general represents the global behavior of the axial capacity.

For all the specimens, the total axial deformation was linear approximately up to the lateral drift angle of 0.6% (1/150). Beyond this point, the different behaviors of axial deformation were shown depending on the applied axial force ratio. For specimens No.1 and No.2-B, on which a lower axial force ratio was applied ( $\eta \geq 0.4$ ), the total axial deformation remained almost constant until that a sudden drop was observed at  $R = 9\%$  or  $7\%$  respectively. For specimens No.2-A and No.3, on which a higher axial force ratio was applied ( $\eta \geq 0.6$ ), the axial deformation became larger as the lateral drift angle increased. For specimen No.3, a sudden drop was observed when the lateral drift angle reached 4.5%, whereas the axial deformation of specimen No.2-A was not observed to drop at any time as it did on the others.

The decreasing tendency of the axial deformation is similar in each specimen in Figure 5. The concentrated compressive axial deformation of portions 5 and 6 (Figure 6) that produced the failure of concrete is reflected in the global axial deformation of Figure 5 for columns No.1, No.2-B and No.3. However, there is a gap between the global axial deformation and the total axial deformation by portions for column No.2-A. One possible reason could be that the distribution of shear and axial deformation in each portion. Compressive axial deformation per portion is distributed in bout edges of the column No.2-A. (Portions 1, 2, 5, 6), and the shear deformation is also better distributed in this column in the portions (2, 3, 4, 5 of Figure 7) in comparison with the rest of the specimens.

Figure 7 shows the shear deformation of each portion. For specimens No.1 and No.2-A, the shear deformation is smaller as compared to the other columns, it can be stated that the failure of specimen No.1 was not caused by shear behavior, and for specimen No.2-A no failure was registered during the test. For specimens No.2-B and No.3, shear deformation on portion 5, which is hinge region, increased drastically at  $R=7\%$  and  $5\%$  respectively. In conjunction with the behavior shown in Figure 5, specimens No.2-B and No.3 failed by shear force at the hinge region at a further lateral drift angle than that of the yielding of hoops of  $R=2\%$ . The ultimate deformation of specimen No.2-B was larger than that of specimen No.3, because the applied axial force of No.2-B was smaller than that of No.3.

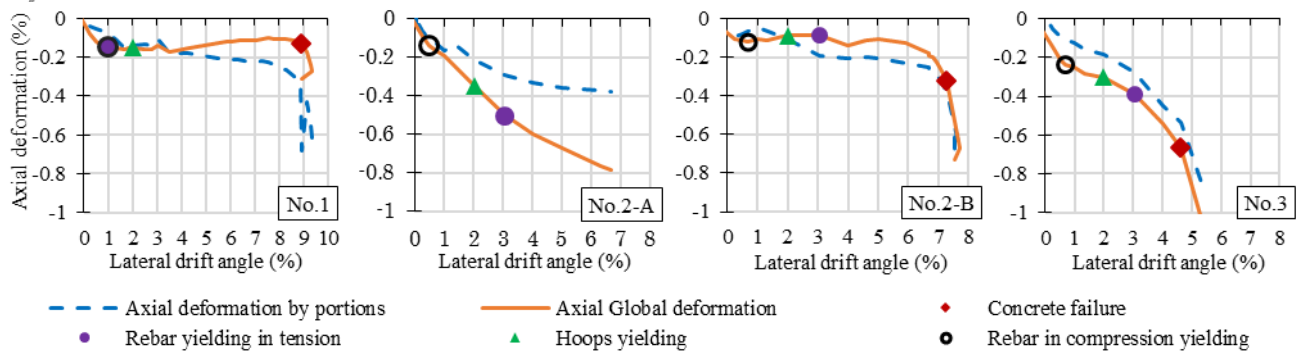


Figure 5 Axial deformation – lateral drift angle relationship

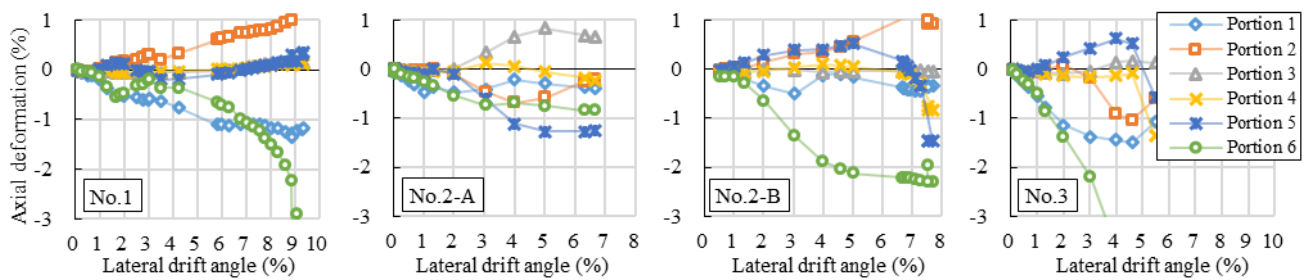


Figure 6 Axial deformation in compression per portion

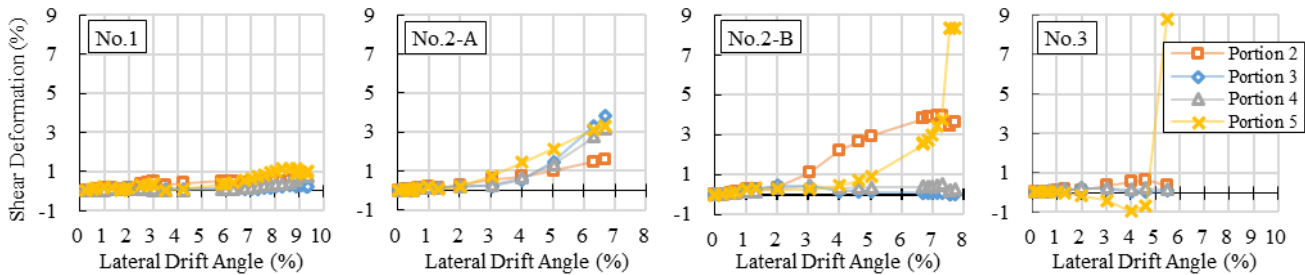


Figure 7 Shear deformation per portion

The failure mode described in the previous paragraphs can be summarized as follows:

Specimen No.1 suffered of axial collapse, given the fact that shear deformation was not dominant as shown in Figure 7.

Specimen No.2-A did not collapse up to the lateral drift angle of 6.7% when the test was finished. However, shear deformation on all portions and axial deformation of member edge (or hinge region) continued increasing as it is shown in Figure 7 and Figure 6 respectively. It is implied that, if lateral loading continues further, portion 5 may be failed by shear manner.

No.2-B and No.3 presented shear failure with axial collapse. The difference on the axial deformation between these columns is due to the applied axial force ratio. The axial deformation was reduced in the same way as the axial force was reduced. In addition, because of the same reason, deformation capacity of No.3 was smaller than that of No.2-B.

All specimens presented a large deformation capacity. However, the specimens loaded with lower axial force ratio, No.1 and No.2-B, collapsed drastically. For the specimens loaded with high axial force ratio, No.3 collapsed drastically and the other, No.2-A, did not collapse but large axial deformation was observed. These characteristics cannot be said to be safe enough.



### 3.3 Deterioration of shear capacity

Given the fact that the arch mechanism satisfies the equilibrium between the truss mechanism and the restoring force characteristics for columns with lower axial force ratio [4], the deterioration of shear capacity ( $V_R$ ) was obtained as the addition of the shear force calculated by truss ( $V_t$ ) and arch mechanism ( $V_a$ ) (Eq. 10). The truss and arch mechanisms were calculated from the strain data recorded during the test by strain gauges placed in the longitudinal and transversal reinforcement (Figure 1). The analysis of this mechanism was carried out in the middle span section of the columns. The reinforcement was considered as a perfectly plastic material, the maximum yielding strength was that shown in Table 3.

$$V_R = V_t + V_a \quad (10)$$

In the next, the equations to obtain the shear capacity is explained. The shear capacity by the truss mechanism was obtained as follow:

$$V_t = p_{we} \sigma_{we} b_e j_e \cot \phi \quad (11)$$

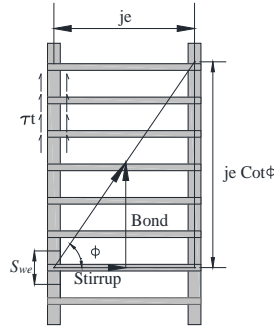


Figure 8 Truss mechanism outline

The angle  $\phi$  is defined as the hypotenuses of the Bond and Stirrup vector forces, the change of the angle  $\phi$  in every step of the test was calculated in base of these forces shown in Figure 8 as follow:

$$\cot \phi = \frac{Bond}{Stirrup}$$

Where the stirrup force is obtained with the strength, the transversal area and the number of bars from each group of stirrups bars.

$$Stirrup\ force = \sigma_{wy} A_s N_s = \varepsilon_s E_{we} A_s N_s$$

Where:  $\sigma_{wy}$  is the strength in the stirrups,  $A_s$  is the transversal area for stirrup,  $N_s$  is the number of stirrup bars,  $\varepsilon_s$  is the average deformation of the recorded data in the stirrups,  $E_{we}$  is the modulus of elasticity of stirrup.

The Bond force is the product of the bond stress ( $\tau_t$ ) multiplied by the total bond area of rebar:

$$Bond = \tau_t S_{we} \phi_B N_B$$

Where:  $\tau_t$  is the bond stress,  $S_{we}$  is the spacing between stirrups,  $\phi_B$  is the diameter on the rebar,  $N_B$  is the number of rebar bars.

The bond stress is defined as follows:

$$\tau_t = \left( \frac{\sigma_y A_B}{h_B \Phi_B} \right) = \left( \frac{\varepsilon_B E_y A_B}{h_B \Phi_B} \right)$$

Where:  $\sigma_y$  is the strength in the rebar,  $A_B$  is the transversal area for rebar,  $h_B$  is the height of the analyzed section,  $\varepsilon_B$  is the average deformation of the recorded data between the edges of the section,  $E_y$  is the modulus of elasticity of rebar,  $\Phi_B$  is the perimeter of the rebar. Then, the Bond force can be written as:

$$Bond = \left( \frac{\varepsilon_B E_y A_B N_B}{h_B \Phi_B} \right) S_{wB} \Phi_B$$

Substituting this equation in the  $\cot \phi$ :

$$\cot \phi = \frac{\left( \frac{\varepsilon_B E_y A_B N_B}{h_B \Phi_B} \right) S_{wB} \Phi_B}{\varepsilon_S E_{wB} A_S N_S}$$

Arranging terms,

$$\cot \phi = \frac{\left( \frac{\varepsilon_B E_y A_B N_B}{h_B \Phi_B} \right)}{\frac{\varepsilon_S E_{wB} A_S N_S}{S_{wB} \Phi_B}}$$

The Bond and Stirrup forces from Figure 8 can be written as follow:

$$Bond = \frac{\varepsilon_B E_y A_B N_B}{h_B \Phi_B} \quad Stirrup = \frac{\varepsilon_S E_{wB} A_S N_S}{S_{wB} \Phi_B}$$

The shear force by arch mechanism ( $V_a$ ) was obtained as follow:

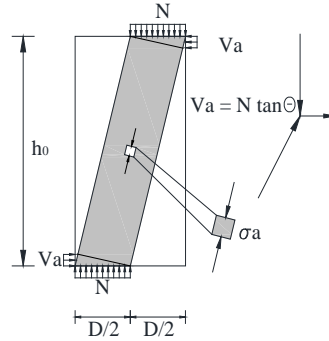


Figure 9 Arch mechanism outline

$$V_a = N_c \tan \theta \quad (12)$$

$N_c = N - N_R$  measured axial force,  $N_c$ : axial force carried by rebar

$$N_R = \sum_i^n A_{Bi} (\varepsilon_{Bi} E_{yi}); \quad \tan \theta = \frac{\frac{D}{2} + \delta_x}{L}$$

Where:  $\delta_x$  lateral displacement (mm) and  $i$  is the number of longitudinal reinforcement bars

Figure 8 presents the outline of the truss and arch mechanism; more details about these mechanisms can be found on references [5].

The deterioration of shear capacity obtained with the truss and arch mechanism was compared with the true shear force ( $Q_{True}$ ) of the test. The true shear force considers the  $P-\delta$  effect of the axial force in this study.

$$Q_{Measured} = Q_{True} - Q_{P-\delta} \quad (13)$$

Where:  $Q_{P-\delta} = \frac{\delta_x}{h_0} N$

Additionally, the shear capacity obtained from these methods is compared to the deterioration of the shear capacity ( $V_u$ ) analyzed with the method published by AIJ [4].



Figure 10 shows the relationship of  $Q_{True}$ ,  $V_u$  and  $V_R$  with the lateral drift angle. In this figure,  $V_u$  from reference 4 predicted the shear degradation with enough safety margin. The truss and arch mechanism well approximated to the true value of shear strength during the test. It can be said that, the method based on the truss and arch mechanism can acceptably predict the deterioration of the shear strength for the selected specimens in this study. A possible reason of the effectiveness of this method could be due to the strong influence of the shear force acting axially along the rebar bars, it means, the recorded strain data is directly originate by the shear force.

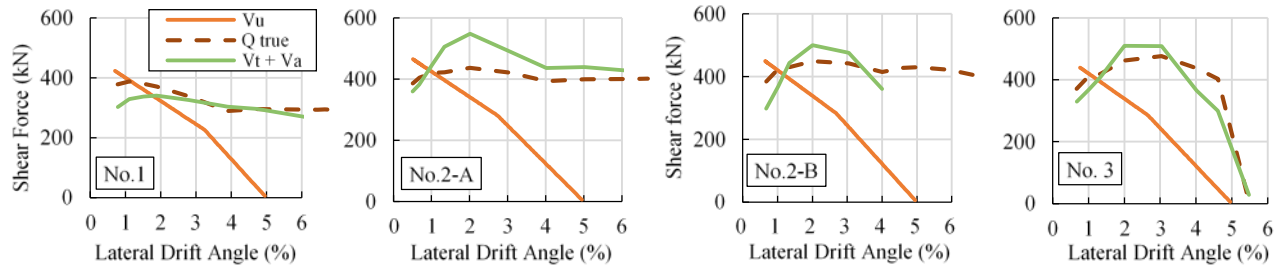


Figure 10 Shear strength deterioration

#### 4. Conclusions

This paper presented a study on the failure mode and shear strength deterioration of four RC columns. The columns were designed to have flexural failure at the beginning of the test. High axial force and cyclic lateral displacement were employed to recreate the seismic effect. At the end of the study, the following conclusions were achieved.

The selected specimens developed desirable deformation capacity, with lateral drift angle larger than 2.5%. For the failure characteristics, most of the specimens collapsed drastically. No. 2-A was the only case that did not collapse. Shear failure and the axial collapse resulted in an important issue for columns No. 2-B and No. 3, the large shear deformation in the hinge regions led the columns to a sudden reduction of the lateral and axial strength. Specimen No. 1 collapsed by the crushing of concrete, which caused the large loss of the axial strength. Specimen No. 2-A did not show any large shear deformation, but given the increasing tendency, it is implied it could also collapse at a larger drift angle. These failure characteristics at the final stage cannot be said to be safe enough for a desirable behavior.

The plastic analysis based on the truss and arch mechanism can predict satisfactorily the deterioration of the shear strength for columns with high axial force. In this study, the compressive strength factor of concrete found from the arch mechanism shows the influence of the axial force. It indicates the importance of its consideration for the methods to predict the degradation of shear strength.

#### 5. References

- [1] Abrams DP (1987): Influence of axial force variations on flexural behavior of reinforced concrete columns, *ACI Structural Journal*, Title no. 84-S26, pp.246-254.
- [2] Architectural Institute of Japan (2014): *Calculation standard for horizontal load-carrying of reinforced concrete structure and comments (For public comments)*, Japan. [http://www.aij.or.jp/jpn/symposium/2014/public\\_20141215.html](http://www.aij.or.jp/jpn/symposium/2014/public_20141215.html).
- [3] Ministry of Land, Infrastructure, Transport, and Tourism (2007): *Technical standard manual concerned to the structure of buildings*, Japan.
- [4] Tasai A and Watanabe A (2000): Residual axial capacity of reinforced concrete columns during shear deterioration, *Japan Concrete Institute Annual Meeting*.
- [5] Architectural Institute of Japan (1999): *Design guidelines for earthquake resistant reinforced concrete building based on inelastic displacement concept*, Japan.



- [6] Kent DC and Park R (1979): Flexural member with confined concrete, *Journal of the Structural Division*, ASCE, Vol. 97 ST7, pp. 1969-1990.
- [7] Ousalem H, Kabeyasawa T, Tasai A, Ohsugi Y (2002): Experimental study on seismic behavior of reinforced concrete columns under constant and variable axial loading, *Japan Concrete Institute*, Vol. 24, No. 2, pp.229-234.
- [8] Okanishi T, Katori K, Hayashi S, Kokusho S. (1994) Deformability of reinforced concrete column subjected to high axial force, *Journal of Structural and Construction Engineering*, AIJ, No. 461, pp.65-74.
- [9] Ishikawa Y, Kimura H (2005): Study on displacement at maximum strength of high strength r/c columns under high axial compression, *Structural Engineering Papers*, AIJ, No. 51B, pp.441-447.